

Observation and explanation of strong electrically tunable exciton g factors in composition engineered In(Ga)As quantum dots

V. Jovanov,^{1,*} T. Eissfeller,¹ S. Kapfinger,¹ E. C. Clark,¹ F. Klotz,¹ M. Bichler,¹ J. G. Keizer,²
P. M. Koenraad,² G. Abstreiter,¹ and J. J. Finley¹

¹Walter Schottky Institut and Physik Department, Technische Universität München, Am Coulombwall 3, D-85748 Garching, Germany

²Department of Applied Physics, Eindhoven University of Technology, P.O. Box 513, NL-5600 MB Eindhoven, The Netherlands

(Received 22 October 2010; published 18 April 2011)

Strong electrically tunable exciton g factors are observed in individual (Ga)InAs self-assembled quantum dots and the microscopic origin of the effect is explained. Realistic eight-band $\mathbf{k} \cdot \mathbf{p}$ simulations quantitatively account for our observations, simultaneously reproducing the exciton transition energy, dc Stark shift, diamagnetic shift, and g factor tunability for model dots with the measured size and a comparatively low In composition of $x_{\text{In}} \sim 35\%$ near the dot apex. We show that the observed g factor tunability is dominated by the hole, with the electron contributing only weakly. The electric-field-induced perturbation of the hole wave function is shown to impact upon the g factor via orbital angular momentum quenching, with the change of the In:Ga composition inside the envelope function playing only a minor role. Our results provide design rules for growing self-assembled quantum dots for electrical spin manipulation via electrical g factor modulation.

DOI: [10.1103/PhysRevB.83.161303](https://doi.org/10.1103/PhysRevB.83.161303)

PACS number(s): 78.67.Hc, 78.20.Jq, 78.55.Cr, 78.60.Fi

The spin of charge carriers in semiconductor quantum dots (QDs) has recently attracted much attention due to the promise it may provide for solid-state quantum information processing.^{1,2} In this respect, the need to selectively rotate a specific spin qubit within a quantum register while simultaneously controlling interactions between spins is challenging. Such selective addressing requires that each qubit has a unique resonance frequency or calls for highly local (≤ 100 nm) time-dependent magnetic fields to selectively rotate a specific qubit.^{3,4} Methods to create nanoscale magnetic fields do not exist, motivating recent proposals for electrical spin control in both single-layer⁵ QDs and QD molecules⁶ via Landé g -tensor modulation. Such approaches aim to tune the magnetic response using electric fields to push the carrier envelope functions into different regions of the nanostructure. This provides the potential to achieve arbitrary spin rotations on the Bloch sphere by applying time-dependent *electric* fields.^{5,6} To date, electrical g factor modulation in semiconductor nanostructures has been demonstrated using parabolically composition graded AlGaAs quantum wells⁷ and vertically coupled (Ga)InAs QD molecules.⁸ However, very weak effects are typically observed for QDs.⁹ Recently, we reported electrically tunable exciton g factors in (Ga)InAs self-assembled QDs grown using the partially covered island (PCI) method. However, due to a lack of information on the microscopic shape and In-composition profile, we could not identify the mechanism responsible for the tuning.¹⁰

In this Rapid Communication, we report very strong electrical tunability of the exciton g factor ($g_{\text{ex}} = g_e + g_h$) in (Ga)InAs self-assembled QDs grown *without* the PCI method and unambiguously identify its microscopic origin. By performing realistic eight-band $\mathbf{k} \cdot \mathbf{p}$ simulations using a QD size, shape, and In composition inferred from scanning tunneling microscopy, we quantitatively account for experimental results and obtain new insight into the origin of the effect. Our experimental and theoretical findings are in excellent agreement; exciton transition energy, dc Stark shift, diamagnetic shift, and g factor tunability all are simultaneously reproduced by theory

using dots with a diameter $D = 25$ nm, height $d = 6$ nm, and a maximum In composition of $x_{\text{In}} \sim 35\%$ near the dot apex. Interestingly, we show that the g_{ex} tunability is dominated by the hole (g_h), with the electron (g_e) contributing only weakly. The electric-field-induced perturbation of the hole envelope wave function is shown to impact upon g_h principally via orbital angular momentum quenching,¹¹ with the change of the In:Ga composition inside the envelope function playing only a minor role. The results show that the strength of the electrical tunability increases as the In-alloy content at the dot apex ($x_{\text{In}}^{\text{apex}}$) is decreased, explaining why we observe strong electrical g_{ex} tunability in our QDs.

The samples investigated were GaAs *n-i*-Schottky photodiode structures grown by molecular beam epitaxy. A single layer of nominally In_{0.5}Ga_{0.5}As self-assembled QDs was grown in the *i* region at an unusually high growth temperature of 595 °C. This is expected to lead to an average In content significantly lower than the nominal value of $x_{\text{In}} = 50\%$, due to the combined effects of In desorption and interdiffusion with the GaAs matrix material during capping.¹² Cross-sectional scanning tunnel microscopy (STM) measurements¹³ performed on high dot density ($> 50 \mu\text{m}^{-2}$) regions of reference samples grown using identical growth conditions revealed dots with a lateral size of 40–50 nm and height of 4–8 nm. In order to estimate the lateral size of the dots from the low density region of the sample ($< 5 \mu\text{m}^{-2}$), we made atomic force microscopy (AFM) measurements at various positions across an uncapped sample grown using the same conditions. These measurements allowed us to directly correlate the variation of local dot diameter across the wafer to the areal density. From the combination of STM and AFM measurements we estimate that the dots studied have a lateral size in the range $D = 18 - 34$ nm and height $h = 4 - 8$ nm.¹⁴

Single dots were optically probed using a low-temperature (4.2 K) magneto-confocal microscope that facilitates application of magnetic (B) fields up to $B = 15$ T in Faraday geometry. Typical photoluminescence (PL) spectra recorded at $B = 10$ T and axial electric fields of 11.4 and 25 kV/cm,

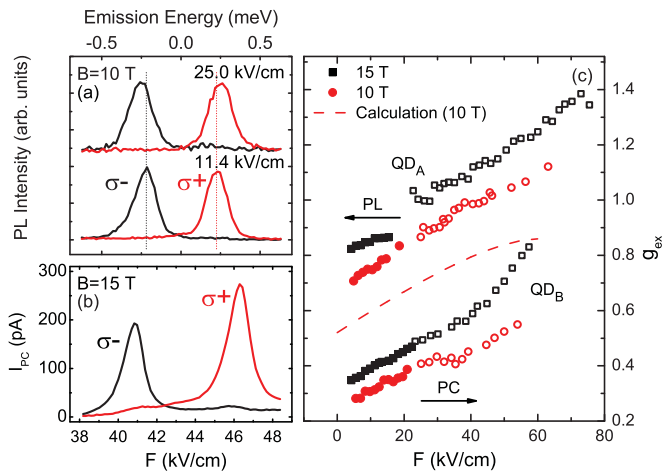


FIG. 1. (Color online) (a) Polarization-resolved photoluminescence spectra at two different electric fields and a magnetic field of 10 T, both applied in the growth direction. To facilitate a direct comparison of the Zeeman gap ($E_Z = g_{ex}\mu_B B$), the Stark shift has been suppressed. (b) Polarization-resolved photocurrent spectra at a magnetic field of 15 T applied in the growth direction. (c) Extracted excitonic g factor as a function of the applied electric field for two representative QDs recorded at 10 T (circles) and 15 T (squares). The dashed line shows the results of eight-band $\mathbf{k} \cdot \mathbf{p}$ calculations using the best-fit dot size and composition parameters described in the text.

respectively, are presented in Fig. 1(a). The results clearly show two Zeeman-split bright excitons with a $\geq 95\%$ degree of circular polarization. Upon increasing the electric field, we observe a clear increase of g_{ex} . For electric fields ≥ 27 kV/cm, the PL quenches due to carrier tunneling from the dot and we probe the energy of the Zeeman branches using polarization-selective photocurrent (PC) absorption measurements. PC spectra recorded with σ^+ and σ^- polarized excitation were obtained at fixed laser frequency, while the levels were tuned into resonance via the dc Stark effect. Typical results are plotted in Fig. 1(b). The dependence of g_{ex} on the electric field is summarized in Fig. 1(c) for two representative QDs labeled QD_A and QD_B. For QD_A, QD_B, and all other dots investigated, g_{ex} increases with the axial electric field.

To understand our results, we performed electronic structure calculations using the eight-band $\mathbf{k} \cdot \mathbf{p}$ envelope function approximation. The magnetic field was introduced into the discrete Hamiltonian in a manifestly gauge-invariant manner^{15,16} and spatial finite-volume discretization, combined with the correct operator ordering, accounted for abrupt material boundaries.¹⁷ Strain fields were included using continuum elasticity theory and their impact on the electronic structure was taken into account via deformation potentials and the linear piezoelectric effect.¹⁸ The direct Coulomb interaction was included in our calculations using lowest-order perturbation theory and the validity of this approximation was carefully checked for a few selected cases where direct electron-hole Coulomb interaction was taken into account in a fully self-consistent manner. To obtain quantitative results for the X^0 energy and g factor, a Luttinger-like eight-band $\mathbf{k} \cdot \mathbf{p}$ model was employed, where far-band contributions to the effective mass Hamiltonian and g factors are included up to

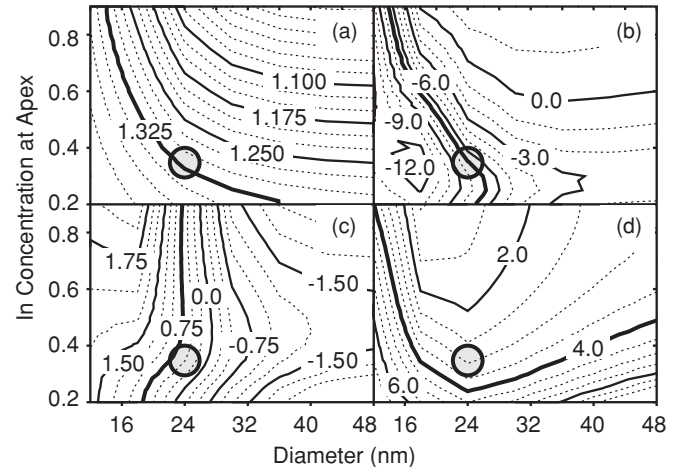


FIG. 2. (Color online) The following properties were obtained by varying QD diameter and InAs content in our calculations: (a) the X^0 exciton energy (eV) at 7 kV/cm and 10 T, (b) the Stark shift energy (meV) between 0 and 60 kV/cm at 10 T, (c) the exciton g factor at zero electric field and 10 T, and (d) the diamagnetic shift energy (meV) between 1 and 13 T at 7 kV/cm. The circles indicate the QD parameters used in the g factor calculations (Fig. 3) and the bold lines indicate experimentally measured values for QD_A.

the order of k^2 .¹⁹ We modeled our QDs as having a truncated lens shape with a diameter D varying from 15 to 50 nm, a height of 6 nm above the wetting layer, and an inverse trumpetlike In-compositional profile.^{20,21} The In concentration of the InGaAs alloy was taken to be $x_{In} = 0.2$ at the base and side of the dot, increasing to $x_{In}^{apex} = 0.2-0.9$ at the dot apex,²¹ parameters that are fully consistent with the results of cross-sectional STM measurements performed on samples grown under the same conditions, from which we also determined the wetting layer thickness (2 nm) and $x_{In}^{WL} = 0.18$.¹³

Figures 2(a), 2(b), and 2(c) show contour plots of the exciton transition energy at 7 kV/cm, Stark shift from 0 to 60 kV/cm, and g_{ex} at $B = 10$ T, respectively. Figure 2(d) shows the diamagnetic shift from 1 to 13 T at an electric field of 7 kV/cm. The measured values of these quantities for QD_A are represented by the bold contours on the figure, showing that all are reproduced in the D , x_{In}^{apex} parameter space probed. More importantly, all of these contours intersect at $D = 24 \pm 2$ nm and $x_{In}^{apex} = 0.35 \pm 0.02$, as indicated by the open circles on the various panels of Fig. 2.²²

The electron and hole g factors in self-assembled dots have been investigated in previous theoretical works, with primary contributions arising from (i) strain-induced band mixing,²³ (ii) modification of Roth's formula by the effective band gap,^{11,24} and (iii) orbital angular momentum quenching.^{11,25,26} Electric-field-induced changes in the alloy overlap, i.e., the In-Ga content within the envelope function, have been shown to be important mostly for very extended electronic states in weakly confined dots.^{11,27} However, while each of the effects (i)–(iii) has been reported to contribute to g_{ex} , the microscopic origin of the strong electrical g_{ex} tunability in our samples is not at all obvious. We now demonstrate that the observed effects can be primarily traced to strong electric-field-induced changes of the hole g factor (g_h), with the electron g factor (g_e) being much more weakly influenced by the electric field. The left

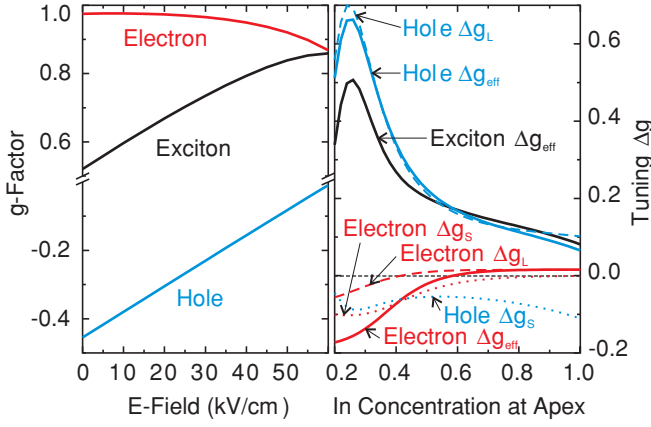


FIG. 3. (Color online) Left: Calculated electron, hole, and exciton g factor as a function of the electric field. Right: Calculated dependency of the electric tuning of g_e , g_h , and g_{ex} as a function of In concentration at the dot apex. The electric tuning is defined as the g factor at 60 kV/cm minus the g factor at 0 kV/cm.

panel of Fig. 3 shows representative calculations of g_h , g_e , and $g_{ex} = g_h + g_e$ for $B = 10$ T using the model dot parameters deduced from Fig. 2 ($D = 24$ nm and $x_{\text{In}}^{\text{apex}} = 0.35$). Clearly, g_e varies only weakly over the range of electric fields investigated ($\Delta g_e/g_e \leq 10\%$), while g_h is much more strongly affected ($\Delta g_h/g_h \geq 50\%$).

We now show that quenching of the orbital angular momentum in zero-dimensional structures [mechanism (iii)] is primarily responsible for the observed electrical tunability. The contributions to the g factor of any electronic state with orbital index n and spin orientation \uparrow or \downarrow ($|n, \uparrow\rangle$ and $|n, \downarrow\rangle$) can be written as²⁵

$$g_n^{\text{eff}} = g_0 + g_{Ln} + g_{Sn}, \quad (1)$$

where $g_0 \approx 2$ is the free-electron Landé g factor and g_{Sn} is the contribution of remote bands included perturbatively in the eight-band $\mathbf{k} \cdot \mathbf{p}$ model, a function of the In content within the envelope function. In comparison, g_{Ln} is the contribution to the g factor due to the angular motion of the electron. We can express g_{Ln} in the framework of first-order perturbation theory,²⁵

$$g_{Ln} = -(\langle n, \uparrow | \hat{L}_z | n, \uparrow \rangle - \langle n, \downarrow | \hat{L}_z | n, \downarrow \rangle), \quad (2)$$

with the orbital angular momentum operator $\hat{L}_z = (\hat{\mathbf{r}} \times \hat{\mathbf{p}})_z$. Equation (2) can be readily evaluated to obtain the tunability of the angular momentum g factor, Δg_L . The right panel of Fig. 3 compares the calculated value of $\Delta g_{e/h} = g_{e/h}(60 \text{ kV/cm}) - g_{e/h}(0 \text{ kV/cm})$ obtained from our full calculation (solid lines, labeled Δg_{eff}) and the contribution Δg_L obtained using Eq. (2) (dashed lines) and the far-band contribution Δg_S (dotted lines) for $0.2 \leq x_{\text{In}}^{\text{apex}} \leq 1.0$.

We find several prominent features of which we highlight two: First, the electric-field tuning of g_h is almost entirely due to the angular momentum contribution. In comparison, g_L plays a much less important role for the electrical modification of g_e . The electrically induced modification of the far-band correction (g_S) is weak for both hole and electron. Second, there is a clear maximum in the tunability of g_h for low In concentrations at the dot apex ($0.25 \leq x_{\text{In}}^{\text{apex}} \leq 0.35$). Thus we

conclude that the observed electrical tunability stems from the modification of the orbital angular momentum of the valence-band state and that the low In content makes the effect so prominent in the presently studied QDs. The increase of the angular momentum contribution g_L to the hole ground state is equivalent to a decrease of angular momentum according to Eq. (2). This quantity can be obtained using second-order perturbation theory and has the following form:

$$g_{Ln} = -\frac{2m_0}{\hbar^2} \sum_{\substack{n' \neq n \\ s'}} \frac{|\langle n, \uparrow | \hat{P}_+ | n', s' \rangle|^2 - |\langle n, \uparrow | \hat{P}_- | n', s' \rangle|^2}{E_n - E_{n'}}, \quad (3)$$

with a momentum operator $\hat{P}_{\pm} = \hat{P}_x \pm i\hat{P}_y$. The sum runs over all conduction and valence-band states $|n', s'\rangle$ except $n' = n$. Here, $\hat{\mathbf{P}} = \frac{1}{\hbar} \partial_{\mathbf{k}} \hat{H}(\mathbf{k})$ is the eight-band momentum operator obtained by the Hellman-Feynman theorem²⁸ and the quantization axis z is taken to be (001), the direction of the applied static magnetic field. While we evaluated Eq. (2) to obtain the Δg_L curves presented in the right panel of Fig. 3, we now make use of Eq. (3) to obtain a qualitative understanding of the observed g_h tunability: The conduction-band (CB) states in a III-V dot have large momentum matrix elements (MMEs), defined by $|\langle n, \uparrow | \hat{P}_{\pm} | n', s' \rangle|^2$ in Eq. (3), with the valence-band (VB) states. In particular, the MME between the lowest-energy electron and hole orbital states without electric field is large. For In-dilute dots there are many bound hole states but only a few bound electron states. For example, we calculate that the best-fit QD from Fig. 2 with $D = 24$ nm and $x_{\text{In}}^{\text{apex}} = 0.35$ accommodates >24 bound hole states, but only 3 bound electron states. The electric field decreases the MME between specific pairs of bound CB and VB orbital states (e.g., lowest orbital states), while this modification is compensated by an increase of the MME between other orbital states due to the completeness of the eigenstates. For the electron ground state, there are many bound hole states available to compensate for the field-induced reduction of the MME between the lowest CB and VB orbital. Each of these VB orbital states has approximately the same relative energy compared to the effective band gap of the dot (~ 1300 meV). Thus the energy denominator of Eq. (3) is approximately the same for each pair of CB and VB states and there is almost no change in the angular momentum of the electron state and a weak tunability of g_e . In strong contrast, for the lowest-energy VB state there are very few bound CB states that can compensate for the field-induced change of the MME. Thus g_h is strongly influenced by the electric field and dominates the observed tunability of g_{ex} .

It has been speculated that the change in alloy overlap may induce heavy hole (HH) - light hole (LH) mixing that could be responsible for the observed strong electrical tunability,¹⁰ since the HH and LH g factors differ strongly. However, our calculations show that ramping the electric field from 0 to 60 kV/cm results in only a weak change of the LH admixture of the lowest VB orbital state ($\approx 0.2\%$). Similarly, the electric field leads to no substantial change of the In:Ga alloy content within the hole envelope function. We calculated that for $x_{\text{In}}^{\text{apex}} = 0.35$ and $D = 24$ nm, the In-alloy overlap changes by $\approx 0.14\%$ or $\approx -2.2\%$ for the hole and electron,

respectively. This leads to an extremely weak change in the far-band correction Δg_S as shown in the right panel of Fig. 3 and does not significantly contribute to the observed electric-field tunability. The results presented in Fig. 3 also show that g_h can be much more widely tuned by varying the static electric field. When coupled with the fact that the hole exhibits weaker hyperfine coupling to the nuclear spin system,²⁹ this observation is particularly relevant from the perspective of hole spin qubits in QD nanostructures.

In summary, we identified the microscopic origin of pronounced electrical tunability of the exciton g factor in (Ga)InAs self-assembled QDs. The g_{ex} tunability was shown

to be dominated by g_h , with g_e contributing only weakly. The electric-field-induced perturbation of the hole envelope wave function was shown to impact upon g_h principally via orbital angular momentum quenching, with the change of the In:Ga composition inside the envelope function playing only a minor role. Our results provide significant scope for morphological and structural tailoring of self-assembled QDs to allow all electrical spin control via the g tensor.⁵

This work is funded by the DFG via SFB-631 and NIM and the EU via SOLID and the TUM Institute for Advanced Study.

*jovanov@wsi.tum.de

- ¹R. Hanson, L. P. Kouwenhoven, J. R. Petta, S. Tarucha, and L. M. K. Vandersypen, *Rev. Mod. Phys.* **79**, 1217 (2007).
- ²O. Gywat, H. J. Krenner and J. Berezovsky, *Spins in Optically Active Quantum Dots* (Wiley-VCH, Berlin, 2010).
- ³F. H. L. Koppens, C. Buizert, K. J. Tielrooij, I. T. Vink, K. C. Nowack, T. Meunier, L. P. Kouwenhoven, and L. M. K. Vandersypen, *Nature (London)* **442**, 766 (2006).
- ⁴M. Kroner, K. M. Weiss, B. Biedermann, S. Seidl, S. Manus, A. W. Holleitner, A. Badolato, P. M. Petroff, B. D. Gerardot, R. J. Warburton, and K. Karrai, *Phys. Rev. Lett.* **100**, 156803 (2008).
- ⁵J. Pingenot, C. E. Pryor, and M. E. Flatté, *Appl. Phys. Lett.* **92**, 222502 (2008).
- ⁶T. Andlauer and P. Vogl, *Phys. Rev. B* **79**, 045307 (2009).
- ⁷G. Salis, Y. Kato, K. Ensslin, D. C. Driscoll, A. C. Gossard, and D. D. Awschalom, *Nature (London)* **414**, 619 (2001).
- ⁸M. F. Doty, M. Scheibner, I. V. Ponomarev, E. A. Stinaff, A. S. Bracker, V. L. Korenev, T. L. Reinecke, and D. Gammon, *Phys. Rev. Lett.* **97**, 197202 (2006).
- ⁹T. Nakaoka, S. Tarucha, and Y. Arakawa, *Phys. Rev. B* **76**, 041301(R) (2007).
- ¹⁰F. Klotz, V. Jovanov, J. Kierig, E. C. Clark, D. Rudolph, D. Heiss, M. Bichler, G. Abstreiter, M. S. Brandt, and J. J. Finley, *Appl. Phys. Lett.* **96**, 053113 (2010).
- ¹¹C. E. Pryor and M. E. Flatté, *Phys. Rev. Lett.* **96**, 026804 (2006).
- ¹²C. Heyn and W. Hansen, *J. Cryst. Growth* **251**, 140 (2003).
- ¹³J. G. Keizer, E. Clark, M. Bichler, G. Abstreiter, J. Finley, and P. Koenraad, *IOP Nanotechnol.* **21**, 215705 (2010).
- ¹⁴D. Pawlizki, Diploma Thesis, Technische Universität München (2008).
- ¹⁵T. Andlauer, R. Morschl, and P. Vogl, *Phys. Rev. B* **78**, 075317 (2008).
- ¹⁶K. G. Wilson, *Phys. Rev. D* **10**, 2445 (1974).
- ¹⁷M. G. Burt, *J. Phys. Condens. Matter* **11**, R53 (1999).
- ¹⁸O. Stier, M. Grundmann, and D. Bimberg, *Phys. Rev. B* **59**, 5688 (1999).
- ¹⁹H. R. Trebin, U. Rössler, and R. Ranvaud, *Phys. Rev. B* **20**, 686 (1979).
- ²⁰P. Offermans, P. M. Koenraad, J. H. Wolter, K. Pierz, M. Roy, and P. A. Maksym, *Phys. Rev. B* **72**, 165332 (2005).
- ²¹M. A. Migliorato, A. G. Cullis, M. Fearn, and J. H. Jefferson, *Phys. Rev. B* **65**, 115316 (2002).
- ²²We note that we also calculated X^0g factors for small ($D \leq 15$ nm), InAs rich (x_{in}^{apex}) dots that are in very good agreement with previous experiments and calculations,²⁷ underscoring the general validity of our theoretical approach.
- ²³T. Nakaoka, T. Saito, J. Tatebayashi, S. Hirose, T. Usuki, N. Yokoyama, and Y. Arakawa, *Phys. Rev. B* **71**, 205301 (2005).
- ²⁴L. Roth, B. Lax, and S. Zwerdling, *Phys. Rev.* **114**, 90 (1959).
- ²⁵A. A. Kiselev, E. L. Ivchenko, and U. Rössler, *Phys. Rev. B* **58**, 16353 (1998).
- ²⁶G. Lommer, F. Malcher, and U. Rössler, *Phys. Rev. B* **32**, R6965 (1985).
- ²⁷T. Nakaoka, T. Saito, J. Tatebayashi, and Y. Arakawa, *Phys. Rev. B* **70**, 235337 (2004).
- ²⁸B. A. Foreman, *J. Phys. Condens. Matter* **12**, R435 (2000).
- ²⁹P. Fallahi, S. T. Yilmaz, and A. Imamoğlu, *Phys. Rev. Lett.* **105**, 257402 (2010).